Evaluating the compressive stress generated during fabrication of Si doubly clamped nanobeams with AFM

Matteo Lorenzoni, Jordi Llobet, Federico Gramazio, Marc Sansa, Jordi Fraxedas, and Francesc Perez-Murano

Citation: Journal of Vacuum Science & Technology B **34**, 06KK02 (2016); doi: 10.1116/1.4967930

View online: https://doi.org/10.1116/1.4967930

View Table of Contents: https://avs.scitation.org/toc/jvb/34/6

Published by the American Vacuum Society

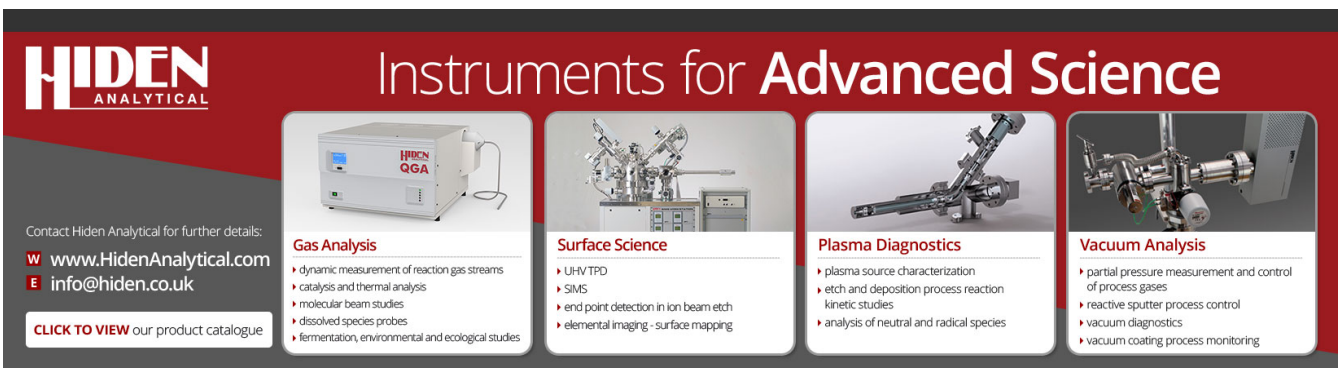

Evaluating the compressive stress generated during fabrication of Si doubly clamped nanobeams with AFM

Matteo Lorenzoni[a] and Jordi Llobet
Institut de Microelectronica de Barcelona, IMB-CNM-CSIC, Campus UAB, 08193 Bellaterra, Spain

Federico Gramazio
Catalan Institute of Nanoscience and Nanotechnology (ICN2), CSIC and The Barcelona Institute of Science and Technology, Campus UAB, 08193 Bellaterra, Spain

Marc Sansa
Institut de Microelectronica de Barcelona, IMB-CNM-CSIC, Campus UAB, 08193 Bellaterra, Spain

Jordi Fraxedas
Catalan Institute of Nanoscience and Nanotechnology (ICN2), CSIC and The Barcelona Institute of Science and Technology, Campus UAB, 08193 Bellaterra, Spain

Francesc Perez-Murano
Institut de Microelectronica de Barcelona, IMB-CNM-CSIC, Campus UAB, 08193 Bellaterra, Spain

(Received 23 June 2016; accepted 3 November 2016; published 15 November 2016)

In this work, the authors employed Peak Force tapping and force spectroscopy to evaluate the stress generated during the fabrication of doubly clamped, suspended silicon nanobeams with rectangular section. The silicon beams, released at the last step of fabrication, present a curved shape that suggests a bistable buckling behavior, typical for structures that retain a residual compressive stress. Both residual stress and Young's modulus were extracted from experimental data using two different methodologies: analysis of beam deflection profiles and tip-induced mechanical bending. The results from the two methods are compared, providing an insight into the possible limitations of both methods.
[http://dx.doi.org/10.1116/1.4967930]

I. INTRODUCTION

Nanometer scale devices have potential applications in multiple areas, and in many cases, their performances are enhanced by their small size or because at the nanometric scale new phenomena appear. For example, within the area of nanomechanics, devices shaped as nanowires or nanobeams have been extensively employed for the creation of high performance mass sensors and integrated oscillators,[1,2] electromechanical resonators,[3] and chemical and biological sensors.[4] Since nanoelectromechanical systems (NEMS) are widely employed in the microelectronic industry, obtaining a reliable quantitative evaluation of the built-in stress induced during the various fabrication steps is crucial to account for changes in the electromechanical properties, like piezoresistive transduction, resonant frequency, or elastic constant. This would eventually allow improving device performances by strain engineering.

Another attracting property in NEMS devices is the mechanical bistable mechanism, in which an element (i.e., a beam) can switch between two configurations and thus exerting a force without consuming power. One of the ways to fabricate such bistable devices is the residual compressive stress buckling.[5,6] The fabrication process we have employed is very likely to introduce such an effect. The hypothesis is here confirmed, and the value of the residual stress at different stages of the fabrication is calculated.

Given the extremely small size of the silicon beams, mechanical measures able to elucidate the buckling mechanism become possible only thanks to AFM measurements. In this work, we study the mechanical deformation of clamped–clamped nanobeams by means of AFM force spectroscopy and Peak Force™ tapping technique with the aim of estimating the residual stress, Young's modulus and confirm the expected bistable behavior. In order to achieve that we compare our experimental data with models picked from present works in literature. With respect to previous works,[7–10] here we investigate silicon suspended nanostructures with rectangular sections.

II. EXPERIMENTAL SECTION

To obtain suspended Si nanobeams, we employed a prototyping method derived from a combination of focused ion beam (FIB) inducing local gallium implantation and selective silicon wet etching, followed by high temperature annealing. The method is described in details elsewhere.[11,12] With this technique, it is possible to create suspended cantilevers, doubly clamped beams,[13] nanopillars,[14] and nanomechanical resonators.[13] The starting substrates are silicon on insulator wafers (⟨110⟩ silicon device layer orientation and thickness $2 \pm 0.5\ \mu$m) while the wet etching employed is a tetramethilammonium hydroxide (TMAH) etching (25% solution at 80 °C) that removes crystalline silicon anisotropically. Amorphous implanted areas defined by FIB are etch-resistant, and moreover, we can exploit the selective etching

[a]Electronic mail: matteo.lorenzoni@imb-cnm.csic.es

rate of TMAH with respect to the crystalline direction to obtain released or nonreleased structures according to their specific orientation. Suspended nanobeams are fabricated by under-etching the silicon below the volume exposed to the FIB. The thickness of the beams is then directly related to the penetration range of the gallium ions in silicon, typically around 40 nm for an ion beam accelerated at 30 keV. As a consequence, the beams are initially made of amorphous silicon doped with gallium. At this moment, the incorporation of high doses of Ga ions produces a considerable distortion of the crystalline lattice. It has been previously documented that materials such as SiO_2 and SiN subjected to kilo-electron-volt ion irradiation develop axial stress if constrained at constant volume.[15] Upon release by under-etching the nonexposed silicon, some of this stress will be released, inducing the curvature of the beam. After the release, an annealing at high temperature (>800 °C) allows to partially recover the crystallinity of the beam and reduces the contents of gallium.

A. Evaluation of the compressive stress

The beams investigated in this work are sketched in Fig. 1(a) (length $l = 4200$ nm; width $w = 550$ nm), beams cross section is assumed to be rectangular, with thickness $t \approx 40$ nm, defined during the ion beam implantation with a tolerance of 5%. The beams' thickness is later measured by SEM; a section image is reported in Fig. 1(b). SEM images of the rectangular doubly clamped beams are reported in Figs. 1(c)–1(e). Clamping areas have structural continuity with the beams. Interestingly, at the end of the fabrication process, the suspended nanobeams present a slight curvature, as visible in Fig. 1(f). We ascribe this phenomenon to the implantation process (the only fabrication step that could introduce a mechanical stress in the structure) and neither to surface stress or displacement of the clamped regions. Accommodating a great number of incoming energetic gallium ions produces a considerable distortion of the original crystalline lattice and even if the gallium ions are removed by the final annealing, the order in the implanted volume of silicon is only partially recovered. The final structure in fact presents nanometer scale grains of polycrystalline silicon containing crystalline defects and twinned silicon structures[16] that are likely to produce a mechanical stress. This stress results to be equivalent to an axial compressive force acting on the beam, whose effect (buckling) is visible only after the release. The final annealing step, as expected, reduces the stress by a certain amount, but still a considerable deformation is visible in the finalized structures. In Fig. 2(a), we report the observed deformation with respect to the horizontal plane (h_0) before and after annealing of beams with different lengths. The curved shape (or self-bending) is visible by SEM [Fig. 1(e)], but electron microscopy is unable to quantify h_0 with the desired accuracy. The

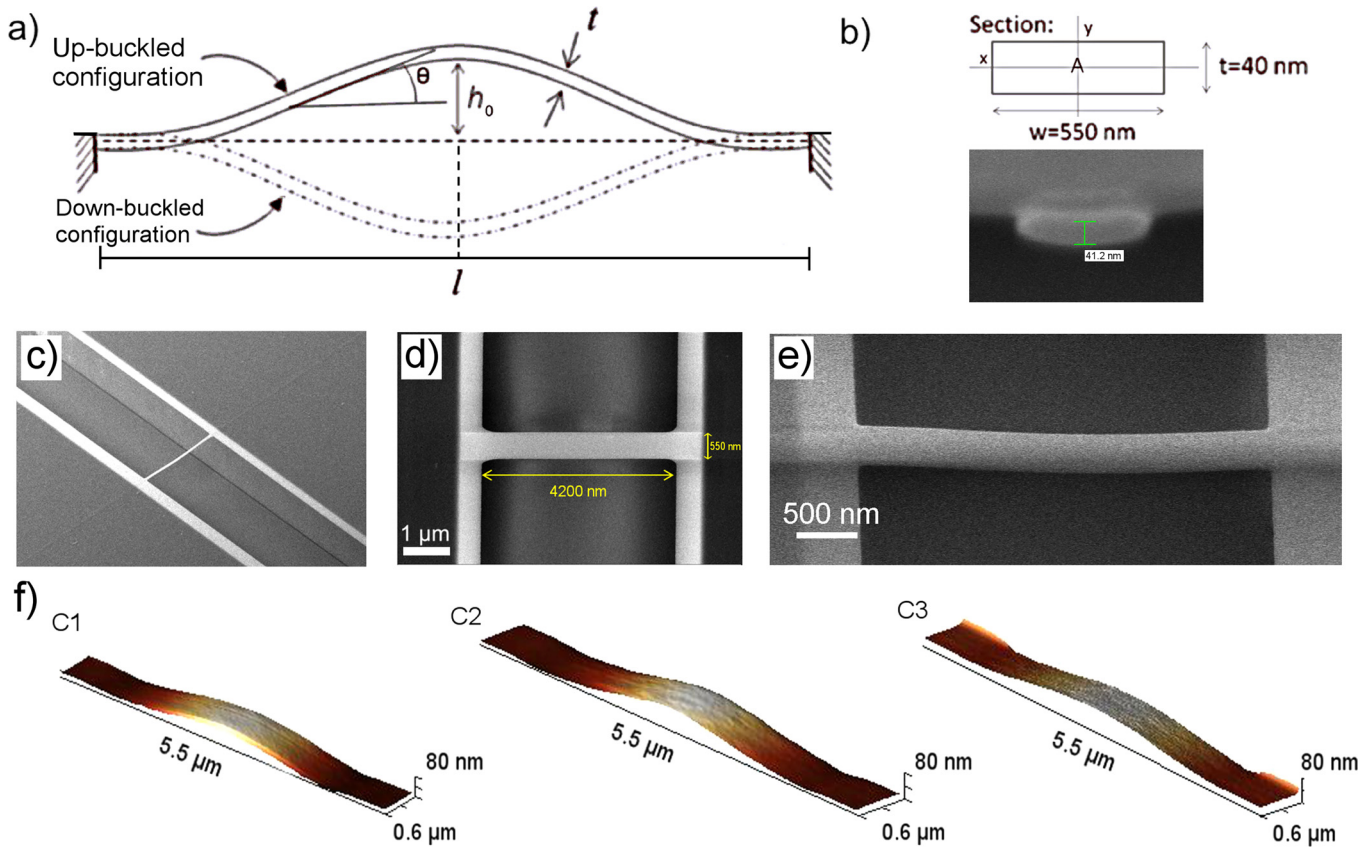

FIG. 1. (Color online) (a) Sketch of the side view of the nanobeam. (b) Beam's section, sketch, and SEM image. [(c)–(e)] SEM images of the fabricated rectangular doubly clamped ultrathin silicon beams. (e) The down-buckling is clearly visible in the image before final annealing. In panel (f), 3D topography of the three beams (C1, C2, and C3) measured by peak force AFM at 1 nN set point force.

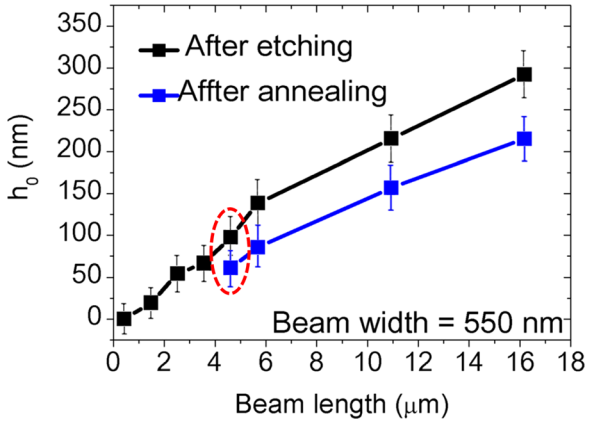

FIG. 2. (Color online) Value of h_0 measured by SEM for beams of different legths after etching (black dotted line) and after subsequent annealing (blue dotted line). The curvature tends to decrease due to the annealing step indicating a partial relaxation of the structure. The red circle highlights the size later measured by AFM.

geometry of the doubly clamped beams is thus measured by peak force AFM [Figs. 1(f) and 3(a)]. By applying a very small constant set point force (approximately 1 nN), the curved configuration is not perturbed; in other words, the force exerted is so small that the beam elastic deformation is negligible and the profile acquired represent the real curved shape. If we increase the load (set point force) during imaging we are able to actuate the beam and switch it from the up-buckled to the down buckled configuration. Considering that once "bended down" the beam holds its new configuration we have a first clear evidence of the bistable instability [Fig. 3(b)]. The beams studied do not present a preferential configuration due the symmetry of the rectangular section. The detailed profile of the symmetric beam C1 in up-buckled position is given in Fig. 3(a). According to the bistable buckled straight-beam mechanism,[17] the minimum axial load P sufficient to buckle a bar with clamped ends is given by

$$P = \frac{4\pi^2 \mathrm{E\,I}}{l^2}, \tag{1}$$

where E is the materials Young's modulus, l is the suspended length, and I is the area momentum of inertia ($\mathrm{I} = \mathrm{wt}^3/12$). The Young's modulus of single crystal Si along the ⟨110⟩ direction is about 170 GPa,[17,18] but it decreases from the value of bulk material when the thickness is reduced into nanometric scale.[20] Moreover, defects cause further decrease in the E value. By measuring the resonant frequency f_o of single clamped beams of the same thickness (40 nm) fabricated with the process here illustrated, it is possible to compare the theoretical and experimental values of f_o determining materials Young's modulus in structures with no residual stress. We thus verified a consistent drop of E in comparison to bulk values (data not shown). Upon those consideration and our experimental findings, we assume a value of $\mathrm{E} = 68$ GPa, as reported in Ref. 20. From Eq. (1), we obtain for the geometry of our symmetric double clamped cantilevers a minimum axial load $\mathrm{P_{min}} = 4.46 \times 10^{-7}$ N. Since we observe a curved

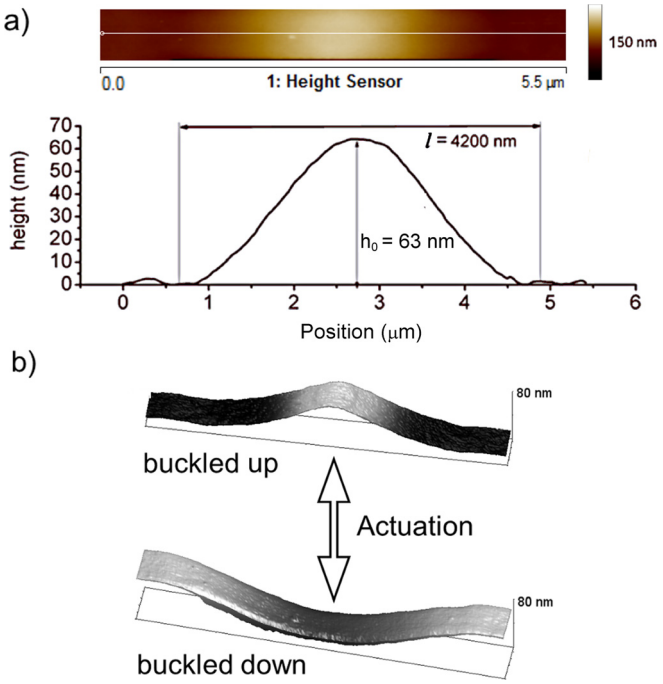

FIG. 3. (Color online) (a) AFM height map of beam C1 in up-buckled position and corresponding height profile. (b) AFM 3D topography of one beam before (up-buckled) and after (down-buckled) actuation.

shape suggesting a buckling, $\mathrm{P_{min}}$ should be compared with the axial stress introduced during fabrication. In order to quantify the axial load able to produce the buckled geometry, we have to consider the difference in elongation between the total length of the beam after buckling, s, and the original length of the compressed beam before it is released, thanks to etching, l. Length s can be found according to the buckled shape imaged in peak force tapping while l (suspended length) is fixed and equal to 4200 nm for all beams. For the three nanobeams considered (C1, C2, and C3 with $h_0 = 63$, 65 and 56 nm, respectively), the elongation is ≈0.05% with s values reported in Table I. Before the release, the axial load ($\mathrm{P^*}$) can be defined by Hook's law[5]

$$P^* = \mathrm{Ewt}\left(\frac{s-l}{l}\right). \tag{2}$$

Taking in consideration only beam C1, given a Young's modulus of 68 GPa, Eq. (2) brings to a value of $\mathrm{P^*} \approx 7.12 \times 10^{-7}$ N, which is enough to create the observed buckling shape of the structures fabricated and geometry measured. The buckling phenomenon implies that part of the stress introduced is released but the structure itself retains a residual stress due to buckling. Evaluating this residual compressive stress, hereafter indicated by σ_1, is possible by using the analytical relationship derived by Luo *et al.*[21] The authors in fact propose an analytical relationship that could directly determine residual stress of clamped SiO_2 microbeams according only to their buckled geometry. The method has been validated for microbeams with larger dimensions (e.g., $60 \times 20\ \mu$m) made of SiO_2; it is therefore interesting to validate the method for ultrathin Si beams. Let us now denote σ_t

TABLE I. Characteristics of the three nanobeams fabricated. σ_1 values obtained from Eq. (5).

Beam	h_0 (nm)	l (nm)	s (nm)	θ (deg)	σ_1 (MPa)
C1	63	4200	4202.1	2.8	22 ± 3.1
C2	65	4200	4202.0	2.9	22 ± 3.1
C3	56	4200	4201.8	2.3	20 ± 2.9

as the compressive residual stress before release, it is related to the axial load P by

$$P = \sigma_t \, \mathrm{w\,t}. \tag{3}$$

Following Ref. 21, we define the uniform compressive stress before release σ_t as the sum of the contribution from elongation and the residual stress σ_1 as follows:

$$\sigma_t = \sigma_1 + \mathrm{E}\left(\frac{s-l}{l}\right), \tag{4}$$

$$\sigma_1 = \frac{8\mathrm{EI}(1-\cos\theta)}{h^2\,\mathrm{w\,t}}, \tag{5}$$

where θ is the maximum angle of deflection [here approximated to the maximum slope of the up-buckled configuration, as in Fig. 1(a)]. Note that the second term of Eq. (4) is Eq. (2) expressed in terms of stress. As elongation occurs, stress is partially relieved and reduced from σ_t to σ_1. Taking in consideration only beam C1 the resulting stress before release $\sigma_t \approx 56$ MPa, obtained combining Eqs. (4) and (5), would lead to a compressive axial force of 1.23×10^{-6} N, approximately three times the minimum load P_{min} needed to obtain a buckling. After being released from the substrate, the nanobeam considered retains a residual compressive stresses due to the buckling deformation $\sigma_1 \approx 22$ MPa. Values of σ_1 for C1, C2, and C3 are reported in Table I.

B. Bending experiments

Once a first estimation of σ_1 from the profile of the buckled beam as measured by AFM was obtained, we can now observe the behavior of the beams when subjected to static deformation, during a three-point bending experiment.[10,19] Three nanobeams have been tested (C1, C2, and C3), the measurements consist of bending experiments performed at the beams' axial center point as depicted in Fig. 4 (deflection is defined as the vertical displacement of the beams center). The experiments start with the beams in the down-buckled configuration [Fig. 4(a)]; the curves obtained are shown in Fig. 4(b). Cantilevers employed were standard Si tapping cantilevers with nominal spring constant of 3 N/m previously calibrated by the thermal tune mehod.[22] It is important to remark that the tip apex was blunt enough not to produce significant indentation on the beam surface during the application of the force to induce the deflection of the beam. As we can see from Fig. 4(b) the plots deviate slightly from linearity. The apparent k of the beams (the slope of the experimental curves) is not constant and tends to increase at increasing deflections.[23] The simplest linear relationship

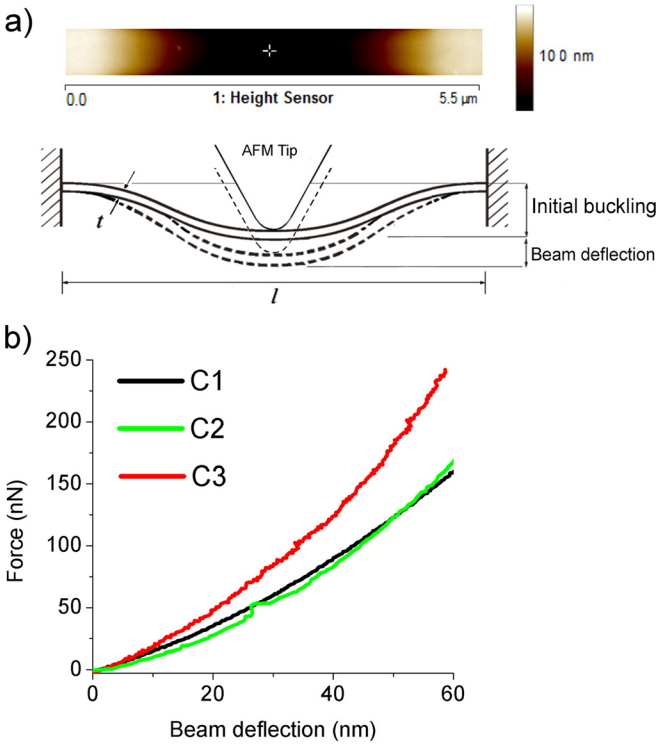

FIG. 4. (Color online) (a) AFM height map of beam C3 in down-buckled position and schematics of an AFM tip exerting a load at the middle of the beam producing a bending. (b) F-D curves from bending experiments on three beams (the starting configuration was down-buckled).The trigger was set at 60 nm displacement. Curves shape is slightly nonlinear, with the apparent k (curve slope) increasing for deflections above 30 nm, as expected for structures with some residual compressive stress.

derived from elastic beam theory that links the exerted force F with the Young's modulus, E, is

$$F = \frac{192\,\mathrm{E}\,I\,d}{l^3}, \tag{6}$$

where d is the beam deflection in the point the force is applied as depicted in Fig. 3(a). Equation (6) is widely used to estimate the Young's modulus of suspended nanostructures[9,24] and holds for deflections that are smaller than the beam's thickness,[19,25] approximately 40 nm for the beams of this study. Beams C1 and C2 present a very similar trend in the first 60 nm of deflection while C3 departs from the other two. This difference is probably due to defect of the under etched area since beam C3 showed a preference after actuation, spontaneously returning to the up-buckled position, as it occurs for beams with triangular section. If we apply this linear approximation in the small displacement range, we obtain overestimated values of the elastic modulus[26] (e.g., $\mathrm{E} \approx 290$ GPa for C1). Since Eq. (6) neglects the effect of any line tension, we need a more complete analytical guess for the F-D curves. To describe such nonlinear behavior during three-point bending experiments,[26] the effect of stress must be taken into account. According to the work of Yaish *et al.*,[10] a good analytical model of the F-D curves for nanobeams with rectangular sections in the small displacement range, $d < 3(w/2)$, is given by the following equation:

$$F = \left(4.8\frac{\sigma^* \mathrm{w\,t}}{l} + 16\frac{\mathrm{E\,w\,t}^3}{l^3}\right)d + 11.52\,\frac{\mathrm{E\,w\,t}}{l^3}d^3. \qquad (7)$$

In this equation, σ^* is positive for tensile residual stress and negative for compressive stress. We fit the experimental data with Eq. (7) having an initial guess for the two fitting parameters (E and σ^*) close to the values calculated in Sec. II A. Since no analytical equation accounting for beams of small profile curvatures is available,[19] we adopt Eq. (7) considering the beam straight, assuming that the initial curvature is not influencing the bending experiment. Interestingly, if we impose $\sigma^* < 0$ (compressive stress), the model is not converging, with best fitting obtained for unrealistic values of E and σ^* approaching zero. If we impose positive values of $\sigma^* > 0$, Eq. (7) tends to reproduce the experimental F-D data. Due to the unavoidable differences occurred during the fabrication steps, the response to bending is different for the three. Beam C1 shows an excellent fit ($R^2 = 0.9985$) for E = 64 GPa and $\sigma^* = 57$ MPa. Fitting are less accurate for beams C2 and C3 when imposing the same value of E = 64 GPa; much better fit quality is obtained allowing E values between 70 and 100 GPa. Fits could be further improved by introducing initial Young's modulus over 100 GPa, but it is unlikely to have such modulus variability within the same fabrication batch. Since the beams are clearly bended and do retain a compressive stress, the outcome of the fittings to Eq. (7) has to be either discarded or better explained. Ignoring the curved shape of our structures is likely to be a too drastic approximation, leading to the conclusion that new models incorporating buckling are needed. Supplementary tests on beams of different geometries might be able to elucidate that aspect. Finally, it is worth to compare values of σ_1 to the outcome of simulations performed in Ref. 13 on beams similar to the ones studied in this work. The simulated model has been varied to fit the experimental values of the resonance frequencies. The dynamic simulation accounts for the effect of the presence of a prestress in the structure producing buckling. The final fit of the model predicts a residual stress of 54 MPa for a predeflection of the beam of 100 nm, a value that is comparable to what measured by the AFM method imaging the profile of the buckled beam.

III. CONCLUSIONS

It has been shown how AFM force spectroscopy combined with Peak Force tapping can provide comprehensive information about ultrathin doubly clamped nanobeams. By combining experimental data with existing models from the literature, we were able to determine the residual stress of Si ultrathin suspended structures. Estimations based on the geometry of the buckled double clamped beam present a simple experimental procedure but needs a known value of material Young's modulus. Three point bending deformation experiments would be able to provide both residual stress and material Young's modulus only if the models available would be adapted, taking into account the initial buckling. Fittings of available models to experimental data are not satisfactory if the expected compressive stress (producing a modest buckling of the structure) is imposed.

ACKNOWLEDGMENTS

The research leading to these results received funding from the European Union's Seventh Framework Programme FP7/2007-2013, under Grant Agreement No. 318804 (SNM). Support is also acknowledged from project Force for future (CSD2010-00024). This work has also been fulfilled in the framework of the Ph.D. school in Physics of the Universitat Autònoma de Barcelona. ICN2 acknowledges support from the Severo Ochoa Program (MINECO, Grant No. SEV-2013-0295).

[1] L. Nicu, *Resonant MEMS* (Wiley-VCH, Weinheim, 2015), pp. 203, 231.
[2] H. G. Craighead, Science **290**, 1532 (2000).
[3] X. L. Feng, R. He, P. Yang, and M. L. Roukes, Nano Lett. **7**, 1953 (2007).
[4] Y. Cui, Q. Wei, H. Park, and C. M. Lieber, Science **293**, 1289 (2001).
[5] J. Qiu, J. H. Lang, and A. H. Slocum, J. Microelectromech. Syst. **13**, 137 (2004).
[6] M. Vangbo and Y. Bäcklund, J. Micromech. Microeng. **8**, 29 (1999).
[7] G. Pennelli, M. Totaro, and A. Nannini, ACS Nano **6**, 10727 (2012).
[8] A. S. Paulo, J. Bokor, and R. T. Howe, Appl. Phys. Lett. **87**, 2003 (2005).
[9] H. Ni, X. Li, and H. Gao, Appl. Phys. Lett. **88**, 043108 (2006).
[10] Y. E. Yaish, Y. Calahorra, O. Shtempluck, and V. Kotchetkov, J. Appl. Phys. **117**, 164311 (2015).
[11] J. Llobet, M. Sansa, M. Gerbolés, N. Mestres, J. Arbiol, X. Borrisé, and F. Pérez-Murano, Nanotechnology **25**, 135302 (2014).
[12] G. Rius, J. Llobet, X. Borrise, N. Mestres, A. Retolaza, S. Merino, and F. Perez-Murano, J. Vac. Sci. Technol., B **27**, 2691 (2009).
[13] J. Llobet, M. Sansa, M. Lorenzoni, X. Borrisé, A. San Paulo, and F. Pérez-Murano, Appl. Phys. Lett. **107**, 073104 (2015).
[14] J. Llobet, M. Sansa, X. Borrisé, F. Pérez-Murano, and M. Gerbolés, Proc. SPIE **9423**, 94230K (2015).
[15] Y. R. Kim, P. Chen, M. J. Aziz, D. Branton, and J. J. Vlassak, J. Appl. Phys. **100**, 104322 (2006).
[16] J. Arbiol, A. Fontcuberta, I. Morral, S. Estradé, F. Peiró, B. Kalache, P. Roca, I. Cabarrocas, and J. R. Morante, J. Appl. Phys. **104**, 064312 (2008).
[17] S. Timoshenko, *Theory of Elastic Stability*, 2nd ed. (McGraw-Hill, New York, 1961), pp. 100, 107.
[18] X. Li, Y. Han, and L. An, Polymer **44**, 8155 (2003).
[19] Y. Calahorra, O. Shtempluck, V. Kotchetkov, and Y. E. Yaish, Nano Lett. **15**, 2945 (2015).
[20] X. Li, T. Ono, Y. Wang, and M. Esashi, Appl. Phys. Lett. **83**, 3081 (2003).
[21] C. Luo, A. Francis, and X. Liu, Microelectron. Eng. **85**, 339 (2008).
[22] J. P. Cleveland, S. Manne, D. Bocek, and P. K. Hansma, Rev. Sci. Instrum. **64**, 403 (1993).
[23] A. Heidelberg, L. T. Ngo, B. Wu, M. A. Phillips, S. Sharma, T. I. Kamins, J. E. Sader, and J. J. Boland, Nano Lett. **6**, 1101 (2006).
[24] B. Varghese *et al.*. Nano Lett. **8**, 3226 (2008).
[25] B. Wu, A. Heidelberg, and J. J. Boland, Nat. Mater. **4**, 525 (2005).
[26] Y.-J. Kim, K. Son, I.-C. Choi, I.-S. Choi, W. Il Park, and J. Jang, Adv. Funct. Mater. **21**, 279 (2011).